THE JOURNAL OF PHYSICAL CHEMISTRY C
A JOURNAL OF THE AMERICAN CHEMICAL SOCIETY

pubs.acs.org/JPCC

Article

Probing the Origin of Photocatalytic Effects in Photothermochemical Dry Reforming of Methane on a Pt/CeO_2 Catalyst

Zichen Du, Fuping Pan, Erik Sarnello, Xuhui Feng, Yang Gang, Tao Li, and Ying Li*

Cite This: https://doi.org/10.1021/acs.jpcc.1c04152

Read Online

ACCESS | Metrics & More | Article Recommendations | Supporting Information

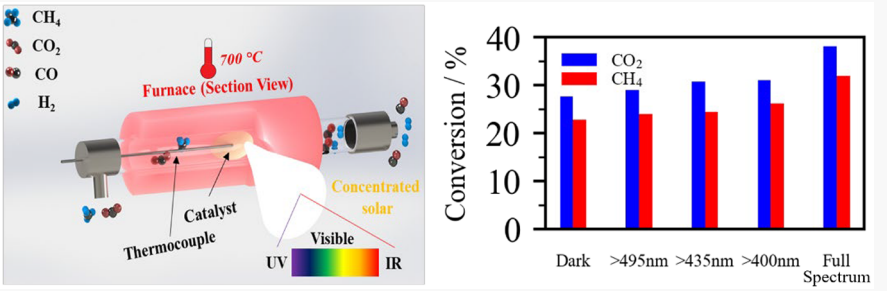

ABSTRACT: Solar-driven photothermochemical dry reforming of methane (PTC-DRM) that integrates thermocatalysis and photocatalysis in one catalyst system is an emerging approach that has demonstrated higher efficiency than thermocatalytic DRM. However, how photocatalysis contributes to the PTC-DRM process at high temperatures remains elusive. Herein, we systematically investigated the photocatalytic effects in PTC-DRM using a photoactive CeO_2-supported Pt catalyst (Pt/CeO_2). The Pt/CeO_2 catalyst showed significant photocatalytic contributions in PTC-DRM, producing CO and H_2 at rates under light irradiation 2.0 and 2.9 times as much as those obtained in the dark at the same temperature, 650 °C. Wavelength-dependence investigation by applying various long-pass filters reveals that the contributions of photocatalysis are mainly from lights less than 435 nm in wavelength, coincident with the band-gap energy of CeO_2, while those longer than 435 nm merely provide heat to drive thermocatalysis. Mechanistic studies from in situ diffuse reflectance infrared Fourier transform spectroscopy (DRIFTS) and from materials characterization before and after the PTC-DRM reaction suggest that photoirradiation regenerates surface oxygen vacancies, thus boosting CO_2 activation and promoting formate and carbonate intermediates conversion to final products. Understanding the photocatalytic effects in PTC-DRM from this work provided insights in designing high-performance catalysts for more efficient solar energy utilization.

1. INTRODUCTION

Significant emissions of greenhouse gases (GHGs) such as carbon dioxide (CO_2) and methane (CH_4) from shale gas reserves, biogas, and landfill gas have been contributing to global warming.[1] Dry reforming of methane (DRM) utilizes CO_2 and CH_4 to produce syngas (CO and H_2), a valuable industrial feedstock to produce liquid fuels through Fischer–Tropsch processes,[2] presenting a promising technology to alleviate the impacts of GHGs. Traditional thermochemical DRM generally requires considerable thermal energy input from burning fossil fuels, which leads to the reemission of GHGs. Instead, solar energy could be a more sustainable and promising energy source to drive DRM.[3−6] The literature has reported a few approaches in solar-assisted DRM.[7] One approach is a solar-driven thermochemical process similar to the traditional thermocatalytic DRM except that concentrated solar energy rather than fossil fuel energy is used to reach the required high temperatures.[6,8] Another approach is operated at room or low temperatures and applies a semiconductor photocatalyst (e.g., titanium dioxide, carbon nitride, tantalum oxynitride, etc.) to exploit high-energy photons in the UV light or near-UV light regions to generate charge carriers for activating DRM.[9−11] The drawback of this process is the low utilization of solar energy as long-wavelength lights are wasted, resulting in low CO and H_2 production rates.

Recently, an integrated photothermochemical DRM (PTC-DRM) has been developed, which incorporates photocatalysis into thermochemical DRM and can significantly boost catalytic activities at high temperatures (600−800 °C) compared to traditional thermo-driven DRM alone.[12−22] The selection of

Received: May 10, 2021
Revised: July 22, 2021

catalysts, either the metal or the support, is vital in determining the exact role of light and corresponding mechanisms in PTC-DRM. In terms of Pt-based catalyst systems for PTC-DRM, there are still discrepancies in the literature regarding the experimental findings and mechanisms with light involvement. Our previous work demonstrated that Pt nanoparticles (NPs) supported on CeO_2 can achieve highly efficient and stable PTC-DRM performance under concentrated solar energy.[12,15] Han et al.[16] reported black TiO_2-supported Pt that can activate DRM by visible-light-driven photocatalysis, but the stability is yet to improve. Liu et al.[14] also suggested the electron−hole-mediated photocatalytic effect in DRM under visible light irradiation at 500 °C on a Pt/TaN catalyst via both experimental and DFT calculations. On the other hand, Mao et al. reported that the activity of a Pt/CeO_2 nanorod catalyst under concentrated solar energy originated from light-driven thermocatalysis and surface plasmon resonance effects of Pt NPs.[20] Their conclusion was based on the experimental findings that activities decreased in a cascade manner when applying different long-pass filters (>420, >560, and >690 nm), but they did not maintain the operating temperature when filtering out short-wavelength light, making it challenging to discover the exact light contributions since DRM activities would change with temperature.[23] Nevertheless, the origin of the photocatalytic effects, if any, and how the experimental parameters such as reaction temperature, light intensity, and light wavelength would influence those effects have not been systematically studied. Furthermore, there is a lack of studies on the activation of reactants and the evolution of intermediates during the PTC-DRM reaction through in situ spectroscopic approaches.

In this work, we aimed to conduct a more systematic exploration of the photocatalytic effects in PTC-DRM over a CeO_2-supported Pt NPs catalyst (Pt/CeO_2). The catalytic DRM performance of Pt/CeO_2 was measured under light irradiation and in the dark at various temperatures, which was further compared to that of ZrO_2-supported Pt (Pt/ZrO_2) as a photoinactive control. To study wavelength-dependence characteristics, three long-wavelength pass filters (495, 435, and 400 nm) were applied to cut off short-wavelength light, and PTC-DRM activities were measured at 700 °C with the corresponding light condition. Moreover, in situ diffuse reflectance infrared Fourier transform spectroscopy (in situ DRIFTS) with light on−off experiments under different filters was performed to understand the photocatalytic effects toward the generation and conversion of reaction intermediates on Pt/CeO_2.

2. METHODS

2.1. Catalyst Synthesis. CeO_2 was prepared by a modified sol−gel method.[12] A surfactant solution was prepared by dissolving 5 mmol of cetyltrimethylammonium bromide (CTAB) in 15 mL of ethanol with sonication until the white powder was fully dissolved. A precursor solution was prepared by dissolving 5 mmol of $Ce(NO_3)_3{\cdot}6H_2O$ and 5 mmol of citric acid in 5 mL of ethanol. The precursor solution was then added dropwise into the surfactant solution under stirring at room temperature. After stirring for another 4 h, the mixed solution was transferred to the oven at 60 °C to age until ethanol was completely dried. The dried gel was then calcined in the air at 500 °C for 5 h at a heating rate of 1 °C min^{-1} to crystallize CeO_2 and remove organic precursors. The powder was then obtained and is denoted as CeO_2. ZrO_2 was prepared using the same method as for CeO_2 while using $ZrOCl_2{\cdot}8H_2O$ as the precursor.

Pt/CeO_2 was synthesized by a wet impregnation method. Specifically, 100 mg of as-prepared CeO_2 was dispersed in 5 mL of ethanol under sonication for 5 min and transferred to a hot plate. Then, 4.2 mL of a 0.5 mg mL^{-1} H_2PtCl_6 aqueous solution was added into the above solution. The mixture was stirred under 50 °C until the solvent was completely evaporated, followed by calcination at 500 °C for 2 h with a heating rate of 5 °C min^{-1} to produce the final Pt/CeO_2 catalyst. Pt/ZrO_2 was prepared using the same method by replacing CeO_2 with ZrO_2.

2.2. Catalyst Characterization. The structure and composition of the as-prepared catalysts were characterized by transmission electron microscopy (TEM, JEOL JEM2100F), X-ray photoelectron spectroscopy (XPS, Omicron), X-ray diffraction (XRD, Bruker-AXS D8 Advanced Bragg−Brentano X-ray powder diffractometer), and Raman spectroscopy (Horiba Jobin-Yvon LabRam HR, 633 nm laser source). UV−vis diffuse reflectance spectra were collected by a Hitachi U4100 UV−vis−NIR Spectrophotometer with a Praying Mantis accessory. Because PTC-DRM activity was evaluated after reducing catalysts in a H_2/Ar mixture at 600 °C for 2 h, all catalysts were characterized after the same reduction step.

2.3. PTC-DRM Experiments. As shown in Figure S1, the PTC-DRM reaction was carried out in a tube (22 mm i.d.) reactor system. A 1.2 kW concentrated solar simulator (ScienceTech Inc.) with custom modular optics enclosures provided a controllable continuous concentrated broad spectrum, and a split tube furnace-powered quartz tube reactor (Applied Test Systems) served as the assistive thermal source. Three long-wavelength pass filters (495, 435, and 400 nm, Edmund Optics) can be placed at the exit of the solar simulator to filter corresponding wavelength ranges. When the concentrated solar simulator was operated at 1.2 kW without auxiliary heat from the furnace, the catalyst surface could reach as high as 480 °C. The irradiance spectrum at 1.2 kW is shown in Figure S2a, which was equivalent to around 30 suns. By tuning the power to 400 and 800 W, the irradiance could be adjusted to 10 and 20 suns, respectively (Figure S2b). A window on the quartz tube reactor provided the channel for light irradiation. The quartz catalyst holder consisted of a modified quartz frit (QPD30-0, Technical Glass Products) in the front and a quartz tube with an oval shape of 24 mm × 16 mm and a 45° inclination angle to make sure that the whole surface was illuminated by the concentrated light. A thermocouple (TC) was in direct contacted with the surface of the catalyst and was connected with the furnace to provide feedback to the heating program, thus ensuring the same reaction temperature under light and dark conditions and eliminating the possible local heating effect. The outlet of the reactor was connected to an online gas chromatograph (GC 2010, Shimadzu) equipped with an automated gas valve and a thermal conductivity detector (TCD) to measure CO_2, CO, and H_2 and a flame ionization detector (FID) to measure CH_4. In this work, only CO and H_2 were detected as the products by GC.

In each PTC-DRM experiment, 5 mg of catalyst powder was dispersed in 5 mL of deionized water under ultrasound sonication to form a uniform ink, and then the ink was dropped onto a piece of Whatman Quartz filter paper and placed on the catalyst holder before being transferred into the

https://doi.org/10.1021/acs.jpcc.1c04152
J. Phys. Chem. C XXXX, XXX, XXX−XXX

tube reactor. The reactor was first purged with 150 standard cubic centimeters per minute (sccm) Ar for 30 min to remove air under room temperature, followed by reducing the catalyst under a mixed flow of 23 sccm H_2 and 28 sccm Ar at 600 °C for 2 h. Then the reactor was purged with 150 sccm Ar to remove H_2 residue. After that, the reactant gases 10% CO_2/10% CH_4/80% Ar (Airgas) were introduced into the reactor with a flow rate of 14 sccm.

2.4. In Situ DRIFTS Experiments. In situ DRIFTS spectra were collected on a Nicolet iS50 infrared spectrometer equipped with an MCT detector and a Praying Mantis DRIFTS environmental chamber with a ZnSe window that allows light irradiation from the concentrated solar source through an optical fiber.[15] The maximum allowable operating temperature of the cell was 600 °C. The detailed procedure and results of the in situ DRIFTS experiments are described later in this paper.

3. RESULTS AND DISCUSSION

The morphology and structure of Pt/CeO_2 and Pt/ZrO_2 were characterized by transmission electron microscopy (TEM). The TEM images of Pt/CeO_2 (Figure 1a) and Pt/ZrO_2 (Figure S3a) exhibit aggregated particles with similar particle sizes averaging around 10 nm. High-resolution TEM (HRTEM) images (Figure 1b and 1c for Pt/CeO_2 and Figure S3b and S3c for Pt/ZrO_2) as well as the inverse fast Fourier transform (FFT) reconstruction (Figures 1d for Pt/CeO_2 and Figure S3d for Pt/ZrO_2) further demonstrate that CeO_2 particles have a lattice spacing of 0.32 nm, corresponding to the (111) facet,[12] while the ZrO_2 particles have a lattice spacing of 0.25 nm (Figure S3d), also corresponding to the (111) facet.[24] The Pt NPs with a size of around 2 nm and a typical interplanar lattice spacing of 0.23 nm, corresponding to the (111) facet,[25] were deposited on CeO_2 (Figure 1e) and ZrO_2 (Figure S3e). The Pt particles on Pt/ZrO_2 are more obvious than those on Pt/CeO_2 from the TEM images, which could be due to partial encapsulation of the Pt nanoparticles by CeO_2 because of the stronger interaction between Pt and CeO_2 support.[26,27]

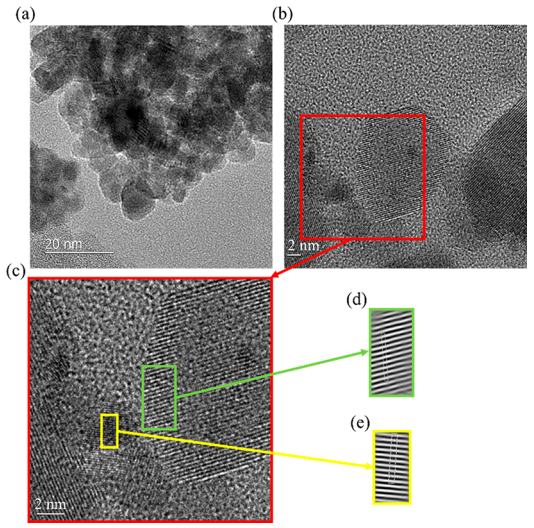

Figure 1. (a) TEM and (b) HRTEM image of Pt/CeO_2, (c) zoomed-in HRTEM image with inverse FFT image regions of Pt and CeO_2, (d) inverse FFT image of CeO_2 in the green region (d spacing = 0.32 nm), and (e) inverse FFT image of Pt in the yellow region (d spacing = 0.23 nm).

The structure of the catalysts was further investigated by X-ray diffraction (XRD) (Figure S4). Pt diffraction peaks were not obvious for both samples, probably due to the low volume fraction. The (111) plane of CeO_2 at 28.6° and (111) plane of ZrO_2 at 28.2° are clearly identified in the XRD and have the typical face-centered cubic fluorite structure, which is in agreement with the TEM results.

The optical properties were measured by UV−vis absorption spectra (Figure 2a), and the band gap was estimated by a Tauc plot using the Kubelka−Munk method (Figure 2b).[28] Pt/ZrO_2 showed relatively weak UV absorption and a large band gap, suggesting that it was not responsive to the UV light, while Pt/CeO_2 exhibited strong UV absorption and had a band gap of 2.84 eV. However, the absorption in the visible light region for Pt/CeO_2 was slightly lower. The surface element composition was further characterized by performing X-ray photoelectron spectroscopy (XPS). The XPS survey spectra in Figure S5 confirm the existence of Pt, O, and support metal. The surface Pt loading of Pt/CeO_2 was measured to be 0.92 wt %, slightly lower than that of Pt/ZrO_2 (1.28 wt %) (Table S1). This may be because some Pt NPs were supported in the bulk of CeO_2 due to the strong interaction between Pt and CeO_2.[20] The relatively low surface Pt amount might be a cause for the weaker visible light absorption of Pt/CeO_2 than Pt/ZrO_2, as the previous report demonstrated that the surface Pt NPs would increase visible light absorption.[29]

We studied DRM behaviors over Pt/CeO_2 under both light irradiation and dark conditions. With the solar simulator operating at 30 suns intensity, the surface temperature on the catalyst was measured to be 480 °C. The equilibrium CO and H_2 production rates were 22.4 and 3.7 mmol g^{-1} h^{-1}, respectively, under light irradiation at 480 °C (Figure S6), while no CO or H_2 peaks were detected in the dark at the same temperature. The observation indicates the positive effects of light to initiate the DRM reaction at a lower temperature, at which the conventional thermocatalytic DRM cannot occur. Furthermore, PTC-DRM experiments were performed by varying reaction temperatures from 500 to 700 °C under both light (30 sun plus auxiliary heat from the furnace) and dark (heat only from the furnace) conditions to investigate the light irradiation contributions at different temperatures. The CO and H_2 production rates and the CO_2 and CH_4 conversion from the 10 h experiments are presented in Figures S7 and S8. The 10 h average values at different temperatures were calculated and are summarized in Figure 3a and 3b. It is clear that the CO and H_2 production rates increase with reaction temperatures under both light and dark conditions, but the difference between light and dark decreases when the temperature was over 650 °C. Specifically, CO and H_2 production rates under light were 2.0 and 2.9 times of those obtained in the dark, respectively, at 650 °C, suggesting the significant contribution from light irradiation to improve the DRM activity. By contrast, CO and H_2 production rates under light condition were 1.4 and 1.6 times those obtained in the dark, respectively, at 700 °C, which further went down to 1.2 and 1.4 times at 750 °C. The decrease in the light contribution at above 650 °C can be attributed to the favorable thermocatalytic DRM at a higher temperature due to the endothermic nature of DRM.[30] It is also noted that the production rates of CO were consistently higher than those of H_2. Since no other products were observed, the higher CO

https://doi.org/10.1021/acs.jpcc.1c04152
J. Phys. Chem. C XXXX, XXX, XXX−XXX

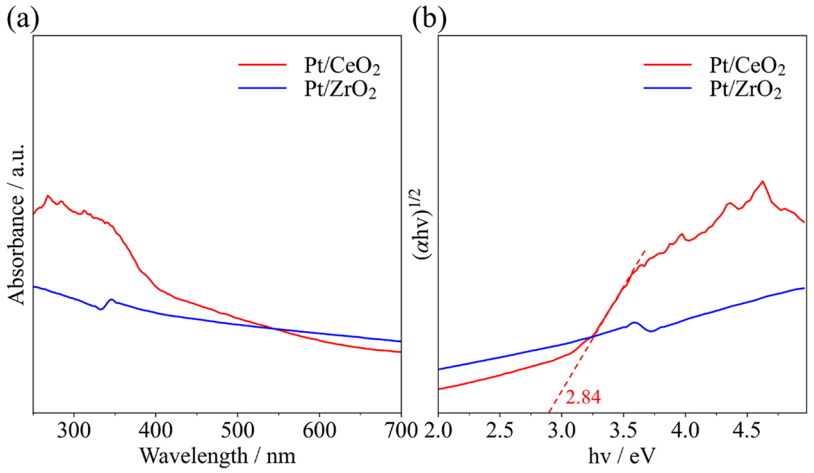

Figure 2. (a) UV−vis absorption spectra and (d) band-gap energies of Pt/CeO_2 and ZrO_2.

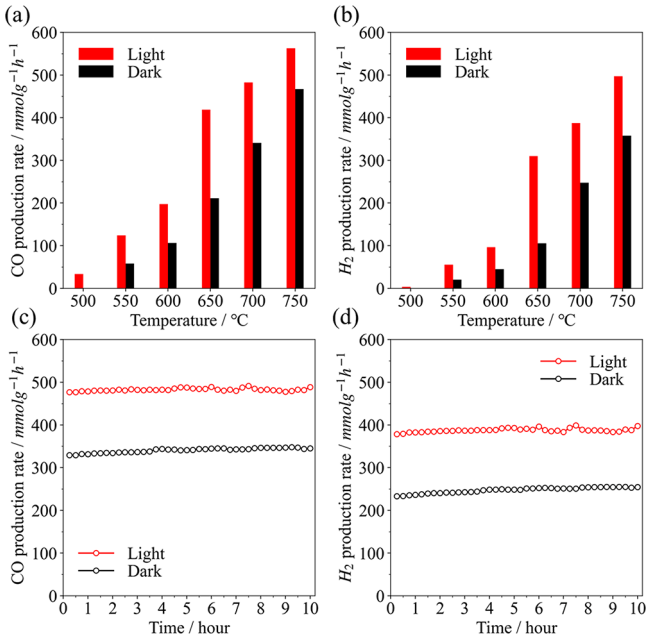

Figure 3. (a and b) Production rates of CO and H_2 on Pt/CeO_2 in the range from 500 to 750 °C under full-spectrum solar irradiation and dark conditions; (c and d) 10 h stability for CO and H_2 production at 700 °C.

production rates might be a result of the occurrence of the reverse water−gas shift (RWGS) reaction ($CO_2 + H_2 \rightarrow CO + H_2O$), which has been widely observed and suggested to be a major side reaction for the lower production rates of H_2 compared to CO in the DRM process.[16,31,32]

The light irradiation intensity was further tuned from 0 to 10, 20, and 30 suns while the temperature was maintained at 700 °C, where 0 sun represents the dark condition. As depicted in Figure S9, both CO and H_2 production rates present a positive linear tendency as the light irradiance increases from 0 to 30 suns, confirming the light-dependent characteristic of PTC-DRM. This linear tendency was also observed in previous works for PTC-DRM on Pt/TaN at 500 °C[14] and Pt−Au/SiO_2 at 400 °C.[18] Considering that the reaction temperature remained unchanged with varying light intensities, the linear relationship between activity and light intensity agrees well with the photocatalytic effect that photoinduced electron−hole pairs actively boost the activity. Moreover, Pt/CeO_2 can maintain a relatively stable DRM performance under both light and dark conditions from 500 to 750 °C (Figures S7 and S8), suggesting that Pt/CeO_2 was able to hinder deterioration, probably due to a stronger metal−support interaction.[33,34]

To further confirm the light contributions from the support to PTC-DRM, DRM activities of Pt/ZrO_2 were measured (Figure S10) and compared to those of Pt/CeO_2, where the Pt loading amount was close to each other. The average CO and H_2 production rates of the 10 h experiment are displayed in Figure 4, and those of CO_2 and CH_4 conversions are in Figure S11. Pt/CeO_2 showed significant enhancements in CO and H_2 production rates under light condition as compared to those in the dark. For Pt/ZrO_2, there are no obvious differences in the CO and H_2 production rates under light and dark conditions, likely because the large band gap of ZrO_2 limited the generation of charge carriers from photocatalysis. The CO and H_2 production rates on Pt/CeO_2 reached 482 and 387 mmol g^{-1} h^{-1} under light condition, which are only 281 and 255 mmol g^{-1} h^{-1} on Pt/ZrO_2, respectively. We further performed PTC-DRM on Pt-free CeO_2 and ZrO_2 supports at 700 °C (Figure 4 and Figure S11). For CeO_2, the CO and H_2 production rates reached 9.9 and 6.9 mmol g^{-1} h^{-1} under light

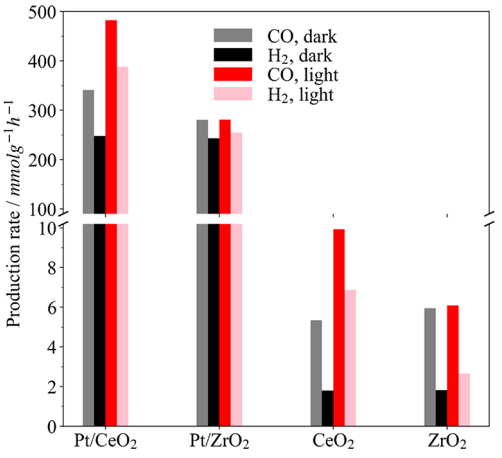

Figure 4. CO and H_2 production rates on Pt/CeO_2, Pt/ZrO_2, CeO_2, and ZrO_2 under full-spectrum solar and in the dark conditions at 700 °C.

https://doi.org/10.1021/acs.jpcc.1c04152
J. Phys. Chem. C XXXX, XXX, XXX−XXX

condition, which are 1.9 and 3.8 times those collected in the dark, verifying the photoactivity of the semiconductor support CeO_2. On the contrary, ZrO_2 yielded 6.1 and 2.1 mmol g^{-1} h^{-1} for CO and H_2 production rates under the light condition, which are almost the same as those obtained in the dark, again verifying the nonphotoactive nature of ZrO_2 under the solar spectrum. The significantly larger yields of Pt-supported catalysts than Pt-free catalysts indicate that the supports alone were not efficiently active and that Pt NPs play critical roles in PTC-DRM, particularly for CH_4 activation.[35] All of the above comparisons demonstrate the important contributions from photocatalysis to the overall PTC-DRM via a photoactive support (e.g., CeO_2).

The spent catalysts after 10 h DRM experiments at 700 °C under the full spectrum and in the dark (Figure S12) were characterized to reveal the possible change in the properties of Pt/CeO_2 under light irradiation. It was found that the average particle size of Pt/CeO_2 was similar under these two conditions. Also, no carbon deposition was observed, as confirmed by the Raman spectroscopy results in Figure S13. Carbon formation was believed to be mainly from the CH_4 dissociation on the metal surface,[36] while a noble metal, like Pt, was demonstrated to have a good carbon resistance. Moreover, the enhanced CeO_2 ability to remove carbon ($2CeO_2 + C \rightarrow Ce_2O_3 + CO$) could be beneficial for strong coke resistance over Pt/CeO_2.[37] Therefore, catalyst sintering, Pt aggregation, and carbon deposition were ruled out as possible reasons for the activity enhancement under the light irradiation. Previous studies suggested that Pt NPs have weak surface plasmon resonance (SPR) effects.[20,38,39] In our case, Pt/ZrO_2 did not show a photoinduced contribution but Pt/CeO_2 did. Thus, Pt-based SPR effects had little contribution to the photocatalytic activity observed in this work.

We then evaluated the possibility that photocatalytic effects would alter the surface property of CeO_2. The surface oxygen vacancy on CeO_2 has been reported to be the site where CO_2 activation happens,[12,15,21] and light irradiance can assist in the desorption of surface oxygen atoms by weakening the metal−oxygen bond and trapping photoexcited electrons on Ce^{4+} to form Ce^{3+} and oxygen vacancies ($Ce^{4+} + e^- \rightarrow Ce^{3+} + V_O$).[40] Since the CO_2 conversion and CO production were lower under dark condition compared with light condition, it is possible that more oxygen vacancies on CeO_2 were generated under light condition. Oxygen vacancies, generally generated by the removal of O atoms at the surface of oxygen carriers, serve as potential sites for reactant adsorption and subsequent activation[41] and provide pathways for oxygen transport through the bulk lattice for surface reaction.[42] For the supports (CeO_2 and ZrO_2), a higher concentration of oxygen vacancies could enhance their reducibility.[43] We measured the Ce 3d chemical states for fresh and spent catalysts by XPS to investigate the change in oxygen vacancies concentration before and after DRM reaction. The pristine and used catalysts were all collected and tested right after the reduction process or DRM at room temperature in an Ar atmosphere to prevent reoxidation by air at high temperatures. As shown in Figure 5, the Ce 3d XPS spectra can be well split into two species, Ce^{4+} and Ce^{3+}, and a larger ratio of $Ce^{3+}/(Ce^{3+} + Ce^{4+})$ represents a higher concentration of oxygen vacancies.[12,44,45] On the basis of the calculated ratios on fresh and spent catalysts, it was found that thermo-driven DRM reactions result in a huge decrease in $Ce^{3+}/(Ce^{3+} + Ce^{4+})$, while under light illumination, the $Ce^{3+}/(Ce^{3+} + Ce^{4+})$ ratio even increases compared to their

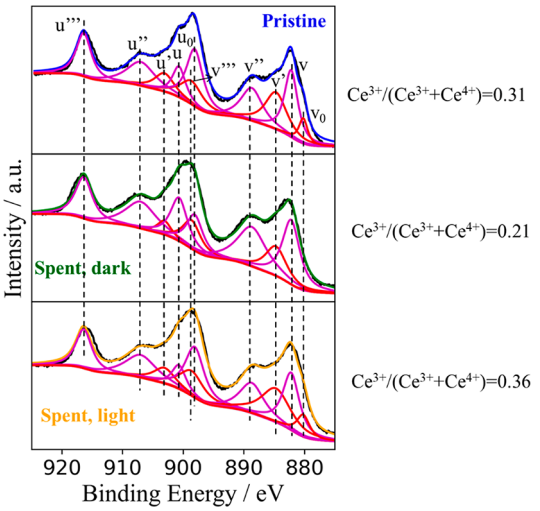

Figure 5. Ce 3d XPS spectra of pristine and spent catalysts after 10 h DRM reaction at 700 °C. u′′′, u′′, u, v′′′, v′′, and v peaks correspond to Ce^{4+}; u′, u0, v′, and v0 peaks corresponds to Ce^{3+}. "Pristine": sample was characterized after H_2 reduction but without the DRM reaction. "Spent, dark": sample was characterized after 10 h DRM reaction in the dark. "Spent, light": sample was characterized after 10 h DRM reaction under light.

initial values, suggesting that oxygen vacancies were generated under light irradiation. On the contrary, the Zr 3d spectra in Figure S14 reveal that Zr maintained a 4+ oxidation state under both light and dark conditions. Therefore, CO_2 activation and reduction could be sustained through the regeneration of oxygen vacancies on Pt/CeO_2, resulting in higher DRM performance under light than in the dark.

To further probe the origin of the photocatalytic effect, we selected Pt/CeO_2 as the model catalyst to study the wavelength-dependent characteristic in PTC-DRM. Since the band gap of 2.84 eV for Pt/CeO_2 corresponds to the cutoff wavelength being 437 nm, we conducted PTC-DRM at 700 °C by applying three long-wavelength pass filters with a cutoff wavelength (495, 435, and 400 nm) longer than, close to, and shorter than that of the absorption edge of Pt/CeO_2, respectively. The PTC-DRM performance of these three groups is presented in Figure 6 and can be compared with Figure 3c and 3d where the dark and full-spectrum activities are displayed. The average values within the 10 h period are also plotted in Figure S15. These results demonstrate that the activities follow the order of full spectrum > 400 nm cutoff > 435 nm cutoff > 495 nm cutoff ≈ dark, the trend of which is especially more apparent for CO_2 conversion. By referring to the light absorption characteristic of CeO_2 (Figure 2a and 2b), the above wavelength-dependent activity data strongly suggest that the origin of the photocatalytic DRM effect is from the band-gap excitation of CeO_2.

Finally, we performed in situ DRIFTS to study the intermediate species during PTC-DRM on Pt/CeO_2 under different light conditions at 600 °C. In order to observe stronger signal changes of the carbonate and formate peaks, the in situ DRIFTS spectra were measured after the CO_2 and CH_4 reaction gases were purged out by Ar gas before conducting the light on/off in situ experiments. The experiment sequence was as follows: (1) the catalyst was first reduced at 600 °C with a mixed flow of 23 sccm H_2 and 28 sccm Ar until no peak change in the spectra was observed; (2) the chamber was then

https://doi.org/10.1021/acs.jpcc.1c04152
J. Phys. Chem. C XXXX, XXX, XXX−XXX

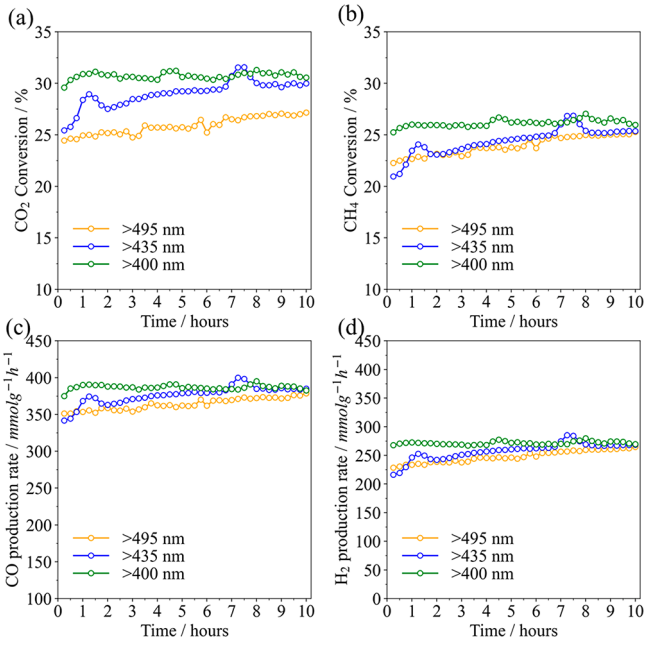

Figure 6. (a) CO_2 and (b) CH_4 conversion and (c) CO and (d) H_2 production on Pt/CeO_2 at 700 °C under solar irradiation with the application of different long-pass filters.

purged with pure Ar to remove remaining H_2 and kept at 600 °C for all following processes; (3) the reactant gases were introduced with a flow rate of 14 sccm until the catalyst was fully saturated with adsorbed species; (4) the chamber was purged with pure Ar to remove reactant gases until the spectra showed no change in order to observe stronger signal changes of potential intermediates in the subsequent light on/off procedures; (5) the chamber was closed and was illuminated, and the spectra were collected for 5 min; (6) the light was turned off, and the spectra were collected for another 5 min. The in situ DRIFTS spectra in the wavenumber range from 1000 to 3000 cm^{-1} for Pt/CeO_2 at 600 °C is illustrated in Figure S16. Other regions except that from 1200 to 1700 cm^{-1} had little changes during the light on/off process, where two strong peaks with observable changes are identified at 1457 and 1374 cm^{-1}, corresponding to unidentate carbonate and formate, respectively.[46] In Figure 7, the evolution of surface-adsorbed species in the region from 1200 to 1700 cm^{-1}, e.g., carbonate and formate, during the light on/off process with the application of different optical filters is presented. Under the full-spectrum solar irradiation condition (Figure 7a), the intensity of the two peaks decreased when illuminated for 0.5 min and decreased further when illuminated for 5 min, indicating the dissociation of the two adsorbed species under the light. When the light was turned off, the intensity of these two peaks increased but could not return to the original level, which suggests readsorption of the two species to a certain extent. With the 400 nm long-pass filter (Figure 7b), the peak intensity decreased but to a lesser degree compared to the full-spectrum illumination when the sample was illuminated for 0.5 min, and the readsorption was not obvious when the light was turned off. With the 435 nm filter (Figure 7c), the peak intensity slightly decreased when the catalyst was illuminated for 0.5 min but remained almost unchanged when the light was off. With the 495 nm filter (Figure 7d), there was almost no difference in the spectra regardless of light on or off. A clear wavelength-dependent tendency can be concluded from the above in situ DRIFTS results, namely, the more UV or near-UV lights in the illumination that serves as the photoexcitation source for CeO_2, the more carbonate and formate intermediates dissociated. A portion of the dissociated intermediates is likely converted to the final CO.[47] However, CO was not observed here, probably because the amount was too small since the gaseous reactants were purged away before the light was illuminated. The in situ DRIFTS results agree with the activity data in Figure 6 that shorter wavelength lights (those shorter than the CeO_2 band-gap excitation cutoff wavelength) contribute most to the enhanced PTC-DRM activity compared to the thermo-DRM alone. By contrast, when in situ DRIFTS light on−off procedure was carried out on Pt/ZrO_2 under full-spectrum solar irradiation (Figure S17), only one strong peak at 1304 cm^{-1} appears, corresponding to bidentate carbonate.[46] Compared to those in the dark, no obvious changes were observed under light, which is consistent with the result that there is no photocatalysis effect by Pt/ZrO_2.

In view of the photocatalysis effects mentioned above, a possible reaction mechanism was proposed as follows. During the PTC-DRM process, CeO_2 was first excited by UV and near-UV lights whose energy is greater than its band-gap energy to generate electron−hole pairs and oxygen vacancies (reactions 1 and 2). In addition to conventional thermocatalytic DRM reaction routes, the photogenerated electron−hole could promote the reaction through the following mechanisms. First, CH_4 dissociation could be boosted by h^+ to generate CH_x and H^+ (reaction 3),[48] where photogenerated electrons could further reduce H^+ to yield H_2 (reaction 4). CH_x is likely converted to C and H^+ as the dissociation reaction progresses. Second, CO_2 dissociation over oxygen vacancies[12] or hydrogenated on CeO_2[47] could be enhanced due to the sustained and even increased number of oxygen vacancies under light illumination, yielding CO, O, carbonate, and formate intermediates (reactions 5 and 6). The produced O is mobile and could help convert C from CH_4 dissociation to CO (reaction 7),[44,49] and the formate species could further decompose into CO (reaction 8). In the overall PTC-DRM process, solar irradiation induces high-energy charge carriers and oxygen vacancies that assist in activating the reactant gases and converting intermediates. Thus, light irradiation could initiate PTC-DRM at a lower temperature and significantly enhance performance compared to the thermo-driven DRM.

$$CeO_2 + h\nu \rightarrow CeO_2 + e^- + h^+ \quad (1)$$

$$Ce^{4+} + e^- \rightarrow Ce^{3+} + V_O + O \quad (2)$$

$$CH_4 + xh^+ \rightarrow CH_x + (4 - x)H^+ \quad (3)$$

$$2H^+ + 2e^- \rightarrow H_2 \quad (4)$$

$$CO_2 + V_O \rightarrow CO \quad (5)$$

$$CO_2 + H^+ + 2e^- \rightarrow HCOO^- \quad (6)$$

$$C + O \rightarrow CO \quad (7)$$

$$HCOO^- + H^+ \rightarrow CO + H_2 \quad (8)$$

4. CONCLUSION

In summary, we probed the photocatalytic effects involved in PTC-DRM over Pt/CeO_2 by comparing the DRM perform-

https://doi.org/10.1021/acs.jpcc.1c04152
J. Phys. Chem. C XXXX, XXX, XXX−XXX

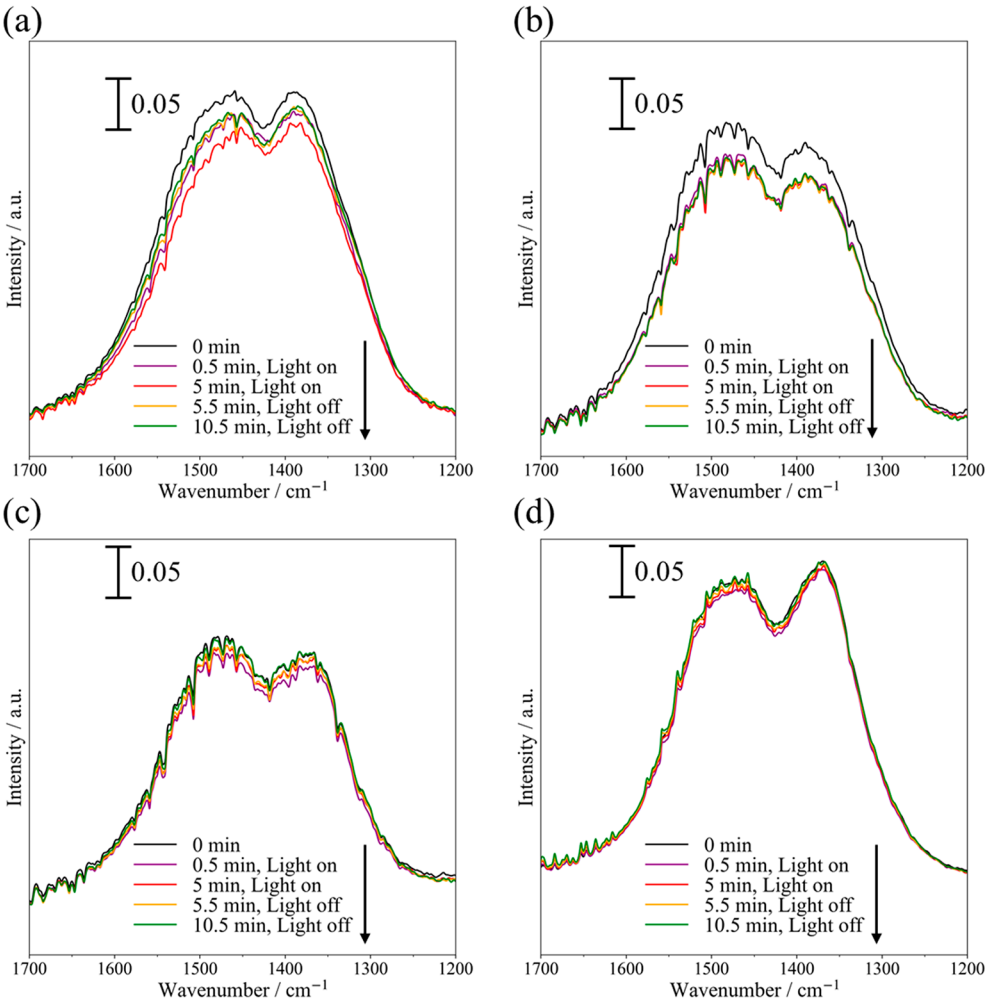

Figure 7. In situ DRIFTS spectra of the Pt/CeO_2 light on−off procedure at 600 °C with (a) full spectrum (no filter), (b) 400 nm filter, (c) 435 nm filter, and (d) 495 nm filter.

ance under light irradiation and dark conditions at a wide range of temperatures. Pt/CeO_2 was an efficient catalyst for PTC-DRM, showing more than doubled catalytic activities under 30 suns irradiation than in the dark. The photocatalytic effects are proved to originate from the semiconductor CeO_2 support through the generation of electron−hole pairs, as evidenced by (1) almost no enhancement in activity when eliminating photons with energy larger than the band gap of CeO_2 using a 435 nm long-pass filter or using a photoinactive ZrO_2 support and (2) photoinduced enhancement in activity proportional to solar intensity when operated at the same temperature. In situ DRIFTS experiments under PTC-DRM reaction conditions and comparison of pre- and postreaction catalyst properties reveal that the photocatalytic effects mainly contribute to (1) inducing the regeneration of oxygen vacancies on CeO_2 that promote CO_2 activation and (2) boosting the conversion of formate and carbonate intermediates, which could be formed at high temperatures via thermocatalytic DRM. As a result, the PTC-DRM performance on Pt/CeO_2 under concentrated solar irradiation is synergistically enhanced compared to thermocatalytic DRM alone.

■ ASSOCIATED CONTENT

Supporting Information

The Supporting Information is available free of charge at https://pubs.acs.org/doi/10.1021/acs.jpcc.1c04152.

Details of calculation of production rates, conversion, reactor configuration, irradiation spectra with different optical filters, additional characterization results including TEM, HRTEM, XRD, XPS, and in situ DRIFTS, and supplemental DRM activity data for both Pt/CeO_2 and Pt/ZrO_2 (PDF)

■ AUTHOR INFORMATION

Corresponding Author

Ying Li − *J. Mike Walker '66 Department of Mechanical Engineering, Texas A&M University, College Station, Texas 77843, United States;* orcid.org/0000-0002-6775-5649; Email: yingli@tamu.edu

Authors

Zichen Du − *J. Mike Walker '66 Department of Mechanical Engineering, Texas A&M University, College Station, Texas 77843, United States;* orcid.org/0000-0002-0231-6944

Fuping Pan − *J. Mike Walker '66 Department of Mechanical Engineering, Texas A&M University, College Station, Texas 77843, United States;* orcid.org/0000-0001-9171-0726

https://doi.org/10.1021/acs.jpcc.1c04152
J. Phys. Chem. C XXXX, XXX, XXX−XXX

Erik Sarnello − *Department of Chemistry and Biochemistry, Northern Illinois University, DeKalb, Illinois 60115, United States*

Xuhui Feng − *J. Mike Walker '66 Department of Mechanical Engineering, Texas A&M University, College Station, Texas 77843, United States*

Yang Gang − *J. Mike Walker '66 Department of Mechanical Engineering, Texas A&M University, College Station, Texas 77843, United States*

Tao Li − *Department of Chemistry and Biochemistry, Northern Illinois University, DeKalb, Illinois 60115, United States; Chemistry and Material Science Group, X-ray Science Division, Argonne National Laboratory, Lemont, Illinois 60439, United States;* orcid.org/0000-0002-4913-4486

Complete contact information is available at: https://pubs.acs.org/10.1021/acs.jpcc.1c04152

Notes

The authors declare no competing financial interest.

■ ACKNOWLEDGMENTS

This work was supported by the U.S. National Science Foundation (Grant Nos. 1924466 and 1924574).

■ REFERENCES

(1) Jang, W. J.; Shim, J. O.; Kim, H. M.; Yoo, S. Y.; Roh, H. S. A review on dry reforming of methane in aspect of catalytic properties. *Catal. Today* **2019**, *324*, 15−26.

(2) Havran, V.; Dudukovic, M. P.; Lo, C. S. Conversion of Methane and Carbon Dioxide to Higher Value Products. *Ind. Eng. Chem. Res.* **2011**, *50* (12), 7089−7100.

(3) Xu, C. Y.; Huang, W. H.; Li, Z.; Deng, B. W.; Zhang, Y. W.; Ni, M. J.; Cen, K. F. Photothermal Coupling Factor Achieving CO2 Reduction Based on Palladium-Nanoparticle-Loaded TiO2. *ACS Catal.* **2018**, *8* (7), 6582−6593.

(4) Liu, L. J.; Zhao, H. L.; Andino, J. M.; Li, Y. Photocatalytic CO2 Reduction with H2O on TiO2 Nanocrystals: Comparison of Anatase, Rutile, and Brookite Polymorphs and Exploration of Surface Chemistry. *ACS Catal.* **2012**, *2* (8), 1817−1828.

(5) Meng, X.; Wang, T.; Liu, L.; Ouyang, S.; Li, P.; Hu, H.; Kako, T.; Iwai, H.; Tanaka, A.; Ye, J. Photothermal conversion of CO2 into CH4 with H2 over Group VIII nanocatalysts: an alternative approach for solar fuel production. *Angew. Chem., Int. Ed.* **2014**, *53* (43), 11478−11482.

(6) Agrafiotis, C.; von Storch, H.; Roeb, M.; Sattler, C. Solar thermal reforming of methane feedstocks for hydrogen and syngas production-A review. *Renewable Sustainable Energy Rev.* **2014**, *29*, 656−682.

(7) Wang, Z. J.; Song, H.; Liu, H. M.; Ye, J. H. Coupling of Solar Energy and Thermal Energy for Carbon Dioxide Reduction: Status and Prospects. *Angew. Chem., Int. Ed.* **2020**, *59* (21), 8016−8035.

(8) Xie, T.; Xu, K. D.; He, Y. L.; Wang, K.; Yang, B. L. Thermodynamic and kinetic analysis of an integrated solar thermochemical energy storage system for dry-reforming of methane. *Energy* **2018**, *164*, 937−950.

(9) Muhammad, A.; Tahir, M.; Al-Shahrani, S. S.; Mahmood Ali, A.; Rather, S. U. Template free synthesis of graphitic carbon nitride nanotubes mediated by lanthanum (La/g-CNT) for selective photocatalytic CO2 reduction via dry reforming of methane (DRM) to fuels. *Appl. Surf. Sci.* **2020**, *504*, 144177.

(10) Tahir, M.; Tahir, B.; Zakaria, Z. Y.; Muhammad, A. Enhanced photocatalytic carbon dioxide reforming of methane to fuels over nickel and montmorillonite supported TiO2 nanocomposite under UV-light using monolith photoreactor. *J. Cleaner Prod.* **2019**, *213*, 451−461.

(11) Cho, Y.; Shoji, S.; Yamaguchi, A.; Hoshina, T.; Fujita, T.; Abe, H.; Miyauchi, M. Visible-light-driven dry reforming of methane using a semiconductor-supported catalyst. *Chem. Commun.* **2020**, *56* (33), 4611−4614.

(12) Pan, F. P.; Xiang, X. M.; Du, Z. C.; Sarnello, E.; Li, T.; Li, Y. Integrating photocatalysis and thermocatalysis to enable efficient CO2 reforming of methane on Pt supported CeO2 with Zn doping and atomic layer deposited MgO overcoating. *Appl. Catal., B* **2020**, *260*, 118189.

(13) Liu, H. M.; Song, H.; Meng, X. G.; Yang, L. Q.; Ye, J. H. Light irradiation enhanced CO2 reduction with methane: A case study in size-dependent optical property of Ni nanoparticles. *Catal. Today* **2019**, *335*, 187−192.

(14) Liu, H. M.; Song, H.; Zhou, W.; Meng, X. G.; Ye, J. H. A Promising Application of Optical Hexagonal TaN in Photocatalytic Reactions. *Angew. Chem., Int. Ed.* **2018**, *57* (51), 16781−16784.

(15) Pan, F. P.; Xiang, X. M.; Deng, W.; Zhao, H. L.; Feng, X. H.; Li, Y. A Novel Photo-thermochemical Approach for Enhanced Carbon Dioxide Reforming of Methane. *ChemCatChem* **2018**, *10* (5), 940−945.

(16) Han, B.; Wei, W.; Chang, L.; Cheng, P. F.; Hu, Y. H. Efficient Visible Light Photocatalytic CO2 Reforming of CH4. *ACS Catal.* **2016**, *6* (2), 494−497.

(17) Liu, H. M.; Li, M.; Dao, T. D.; Liu, Y. Y.; Zhou, W.; Liu, L. Q.; Meng, X. G.; Nagao, T.; Ye, J. H. Design of PdAu alloy plasmonic nanoparticles for improved catalytic performance in CO2 reduction with visible light irradiation. *Nano Energy* **2016**, *26*, 398−404.

(18) Song, H.; Meng, X. G.; Dao, T. D.; Zhou, W.; Liu, H. M.; Shi, L.; Zhang, H. B.; Nagao, T.; Kako, T.; Ye, J. H. Light-Enhanced Carbon Dioxide Activation and Conversion by Effective Plasmonic Coupling Effect of Pt and Au Nanoparticles. *ACS Appl. Mater. Interfaces* **2018**, *10* (1), 408−416.

(19) Liu, H. M.; Meng, X. G.; Dao, T. D.; Liu, L. Q.; Li, P.; Zhao, G. X.; Nagao, T.; Yang, L. Q.; Ye, J. H. Light assisted CO2 reduction with methane over SiO2 encapsulated Ni nanocatalysts for boosted activity and stability. *J. Mater. Chem. A* **2017**, *5* (21), 10567−10573.

(20) Mao, M. Y.; Zhang, Q.; Yang, Y.; Li, Y. Z.; Huang, H.; Jiang, Z. K.; Hu, Q. Q.; Zhao, X. J. Solar-light-driven CO2 reduction by methane on Pt nanocrystals partially embedded in mesoporous CeO2 nanorods with high light-to-fuel efficiency. *Green Chem.* **2018**, *20* (12), 2857−2869.

(21) Shoji, S.; Peng, X. B.; Yamaguchi, A.; Watanabe, R.; Fukuhara, C.; Cho, Y.; Yamamoto, T.; Matsumura, S.; Yu, M. W.; Ishii, S.; Fujita, T.; Abe, H.; Miyauchi, M. Photocatalytic uphill conversion of natural gas beyond the limitation of thermal reaction systems. *Nat. Catal* **2020**, *3* (2), 148−153.

(22) Liu, H. M.; Meng, X. G.; Dao, T. D.; Zhang, H. B.; Li, P.; Chang, K.; Wang, T.; Li, M.; Nagao, T.; Ye, J. H. Conversion of Carbon Dioxide by Methane Reforming under Visible-Light Irradiation: Surface-Plasmon-Mediated Nonpolar Molecule Activation. *Angew. Chem., Int. Ed.* **2015**, *54* (39), 11545−11549.

(23) Abdulrasheed, A.; Jalil, A. A.; Gambo, Y.; Ibrahim, M.; Hambali, H. U.; Shahul Hamid, M. Y. A review on catalyst development for dry reforming of methane to syngas: Recent advances. *Renewable Sustainable Energy Rev.* **2019**, *108*, 175−193.

(24) Lu, Y. W.; Shieh, J.; Tsai, F. Y. Induction of ferroelectricity in nanoscale ZrO2/HfO2 bilayer thin films on Pt/Ti/SiO2/Si substrates. *Acta Mater.* **2016**, *115*, 68−75.

(25) Yu, L.; Shao, Y.; Li, D. J. A. C. B. E. Direct combination of hydrogen evolution from water and methane conversion in a photocatalytic system over Pt/TiO2. *Appl. Catal., B* **2017**, *204*, 216−223.

(26) Du, J. S.; Bian, T.; Yu, J.; Jiang, Y.; Wang, X.; Yan, Y.; Jiang, Y.; Jin, C.; Zhang, H.; Yang, D. Embedding Ultrafine and High-Content Pt Nanoparticles at Ceria Surface for Enhanced Thermal Stability. *Adv. Sci. (Weinh)* **2017**, *4* (9), 1700056.

(27) Lee, S.; Seo, J.; Jung, W. Sintering-resistant Pt@CeO2 nanoparticles for high-temperature oxidation catalysis. *Nanoscale* **2016**, *8* (19), 10219−28.

(28) Rao, G. Y.; Zhao, H. L.; Chen, J. T.; Deng, W.; Jung, B.; Abdel-Wahab, A.; Batchelor, B.; Li, Y. FeOOH and Fe2O3 co-grafted TiO2

photocatalysts for bisphenol A degradation in water. *Catal. Commun.* **2017**, *97*, 125−129.
(29) Pastor-Perez, L.; Ramos-Fernandez, E. V.; Sepulveda-Escribano, A. Effect of the CeO2 synthesis method on the behaviour of Pt/CeO2 catalysis for the water-gas shift reaction. *Int. J. Hydrogen Energy* **2019**, *44* (39), 21837−21846.
(30) Pakhare, D.; Spivey, J. A review of dry (CO2) reforming of methane over noble metal catalysts. *Chem. Soc. Rev.* **2014**, *43* (22), 7813−7837.
(31) Kattel, S.; Liu, P.; Chen, J. G. G. Tuning Selectivity of CO2 Hydrogenation Reactions at the Metal/Oxide Interface. *J. Am. Chem. Soc.* **2017**, *139* (29), 9739−9754.
(32) Wang, N.; Qian, W. Z.; Chu, W.; Wei, F. Crystal-plane effect of nanoscale CeO2 on the catalytic performance of Ni/CeO2 catalysts for methane dry reforming. *Catal. Sci. Technol.* **2016**, *6* (10), 3594−3605.
(33) Farmer, J. A.; Campbell, C. T. Ceria Maintains Smaller Metal Catalyst Particles by Strong Metal-Support Bonding. *Science* **2010**, *329* (5994), 933−936.
(34) Singha, R. K.; Yadav, A.; Shukla, A.; Kumar, M.; Bal, R. Low temperature dry reforming of methane over Pd-CeO2 nanocatalyst. *Catal. Commun.* **2017**, *92*, 19−22.
(35) Nagaoka, K.; Seshan, K.; Aika, K.; Lercher, J. A. Carbon deposition during carbon dioxide reforming of methane - Comparison between Pt/Al2O3 and Pt/ZrO2. *J. Catal.* **2001**, *197* (1), 34−42.
(36) Muraza, O.; Galadima, A. A review on coke management during dry reforming of methane. *Int. J. Energy Res.* **2015**, *39* (9), 1196−1216.
(37) Jones, J.; Xiong, H.; DeLaRiva, A. T.; Peterson, E. J.; Pham, H.; Challa, S. R.; Qi, G.; Oh, S.; Wiebenga, M. H.; Pereira Hernandez, X. I.; Wang, Y.; Datye, A. K. Thermally stable single-atom platinum-on-ceria catalysts via atom trapping. *Science* **2016**, *353* (6295), 150−154.
(38) Zhang, N.; Han, C.; Xu, Y. J.; Foley, J. J.; Zhang, D. T.; Codrington, J.; Gray, S. K.; Sun, Y. G. Near-field dielectric scattering promotes optical absorption by platinum nanoparticles. *Nat. Photonics* **2016**, *10* (7), 473−482.
(39) Bigall, N. C.; Hartling, T.; Klose, M.; Simon, P.; Eng, L. M.; Eychmuller, A. Monodisperse Platinum Nanospheres with Adjustable Diameters from 10 to 100 nm: Synthesis and Distinct Optical Properties. *Nano Lett.* **2008**, *8* (12), 4588−4592.
(40) Dulub, O.; Batzilln, M.; Solovev, S.; Loginova, E.; Alchagirov, A.; Madey, T. E.; Diebold, U. J. S. Electron-induced oxygen desorption from the TiO2 (011)-2× 1 surface leads to self-organized vacancies. *Science* **2007**, *317* (5841), 1052−1056.
(41) Esch, F.; Fabris, S.; Zhou, L.; Montini, T.; Africh, C.; Fornasiero, P.; Comelli, G.; Rosei, R. Electron localization determines defect formation on ceria substrates. *Science* **2005**, *309* (5735), 752−755.
(42) Mihai, O.; Chen, D.; Holmen, A. Catalytic Consequence of Oxygen of Lanthanum Ferrite Perovskite in Chemical Looping Reforming of Methane. *Ind. Eng. Chem. Res.* **2011**, *50* (5), 2613−2621.
(43) Mihai, O.; Chen, D.; Holmen, A. Chemical looping methane partial oxidation: The effect of the crystal size and O content of LaFeO3. *J. Catal.* **2012**, *293*, 175−185.
(44) Xiang, X. M.; Zhao, H. H.; Yang, J.; Zhao, J.; Yan, L.; Song, H. L.; Chou, L. J. Nickel based mesoporous silica-ceria-zirconia composite for carbon dioxide reforming of methane. *Appl. Catal., A* **2016**, *520*, 140−150.
(45) Della Mea, G. B.; Matte, L. P.; Thill, A. S.; Lobato, F. O.; Benvenutti, E. V.; Arenas, L. T.; Jurgensen, A.; Hergenroder, R.; Poletto, F.; Bernardi, F. Tuning the oxygen vacancy population of cerium oxide (CeO2-x, $0 < x < 0.5$) nanoparticles. *Appl. Surf. Sci.* **2017**, *422*, 1102−1112.
(46) Jacobs, G.; Williams, L.; Graham, U.; Sparks, D.; Davis, B. H. Low-temperature water-gas shift: in-situ DRIFTS- reaction study of a Pt/CeO2 catalyst for fuel cell reformer applications. *J. Phys. Chem. B* **2003**, *107* (38), 10398−10404.
(47) Ferreira-Aparicio, P.; Rodriguez-Ramos, I.; Anderson, J. A.; Guerrero-Ruiz, A. Mechanistic aspects of the dry reforming of methane over ruthenium catalysts. *Appl. Catal., A* **2000**, *202* (2), 183−196.
(48) Yu, L. H.; Shao, Y.; Li, D. Z. Direct combination of hydrogen evolution from water and methane conversion in a photocatalytic system over Pt/TiO2. *Appl. Catal., B* **2017**, *204*, 216−223.
(49) Huang, T. J.; Lin, H. J.; Yu, T. C. A comparison of oxygen-vacancy effect on activity behaviors of carbon dioxide and steam reforming of methane over supported nickel catalysts. *Catal. Lett.* **2005**, *105* (3−4), 239−247.

https://doi.org/10.1021/acs.jpcc.1c04152
J. Phys. Chem. C XXXX, XXX, XXX−XXX